13th International Symposium on Turbulence and Shear Flow Phenomena (TSFP13)
Montreal, Canada, June 25–28, 2024

TURBULENT SEPARATION DETECTION BASED ON A LAGRANGIAN APPROACH

Motahareh Sadr & Jérôme Vétel
Department of Mechanical Engineering, LADyF
Polytechnique Montreal
Montreal, Quebec, H3T 1J4, Canada
seyedeh-motahareh.sadr@polymtl.ca, jerome.vetel@polymtl.ca

INTRODUCTION

Flow separation is observed in all devices that deal with fluid flows and can cause lift loss, drag increase, transition to instabilities and turbulence or undesired vibrations. Predicting it is the beginning stage of controlling and delaying such an unwelcome occurrence. The pursuit of grasping this phenomenon goes back a long way. It starts with the fundamental work of Prandtl (1904) who developed the notion of boundary layers and specified the separation point in a two-dimensional (2D), incompressible, steady flow as the location on the wall where the skin friction (τ_w) is zero and its longitudinal derivative is negative. In three-dimensional (3D) or unsteady flows, the Prandtl criterion is not valid and many other tools have been and are still proposed until today. For example, Moore (1958), Rott (1956) and Sears (1956) individually suggested what is now known as the MRS criterion, that the separation point is located within the boundary layer where there is no shear and no streamwise velocity component in a frame of reference moving with the separation point, which makes the criterion difficult to apply in practice.

Further numerical studies aimed to capture singularities in the unsteady boundary layer equations. Van Dommelen & Shen (1980, 1982) used Lagrangian coordinates to describe the problem and observed a singularity where the MRS criterion holds. While using Lagrangian coordinates shows an advantage, the method depends strongly on how boundary layer equations are solved, which, again, makes this principle difficult to apply.

Haller (2004) proposed an exact theory for separation in unsteady 2D flows. He called separation a Lagrangian phenomenon and described it as 'the convergence and subsequent ejection of fluid particles from the vicinity of the boundary', and classifying the unsteady separation as either fixed or moving, associated it with material spike in the vicinity of the boundary. This theory was extended to 3D flows for steady and fixed unsteady separation (Surana *et al.*, 2006, 2008). Another approach to detect separation is through material spikes. Serra *et al.* (2018) studied 2D flows and associated the locations of maximum curvature in material lines with spikes. This theory was recently extended to 3D flows as well (Santhosh *et al.*, 2023). These latest studies are very promising, but the methods could be difficult to apply for very complex flows, the extreme case being turbulent separation. This is this case that is considered in this study.

METHODOLOGY

The proposed criterion to capture separation is first introduced by Haller (2011) and employed in a variational theory to extract Lagrangian Coherent Structures. The *repulsion rate* is a measure of assessing perturbation growth in the normal direction of a material surface. In order to define this parameter, consider the following dynamical system:

$$\dot{\mathbf{x}} = \mathbf{u}(\mathbf{x}, t), \tag{1}$$

where $\mathbf{u}$ is the velocity vector field. The initial position of a fluid particle at time t_0 is $\mathbf{x}_0$, and at time t, a trajectory of the system is $\mathbf{x}(t, t_0, \mathbf{x}_0)$. This passage is expressed through the flow map $\mathbf{F}_{t_0}^{t}(\mathbf{x}_0)$. A snapshot of an invariant manifold $\mathcal{M}$ of the system (1) at time t is a material surface $\mathcal{M}(t)$, that is made by advecting initial surface $\mathcal{M}(t_0)$ through the flow map $\mathbf{F}_{t_0}^{t}$:

$$\mathcal{M}(t) = \mathbf{F}_{t_0}^{t}(\mathcal{M}(t_0)), \quad \mathcal{M}(t) \subset \mathbb{R}^n. \tag{2}$$

Now for an arbitrary point $\mathbf{x}_0 \in \mathcal{M}(t_0)$, consider we break it down into a one-dimensional normal space, $N_{\mathbf{x}_0}\mathcal{M}(t_0)$, and a $(n-1)$-dimensional tangent space, $T_{\mathbf{x}_0}\mathcal{M}(t_0)$ (figure 1).

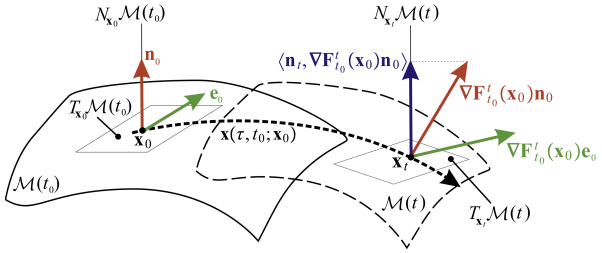

Figure 1. Material surface $\mathcal{M}(t)$ and its geometry (from Haller, 2011)

The tangent space, $T_{\mathbf{x}_0}\mathcal{M}(t_0)$, is transported by the flow map $\nabla \mathbf{F}_{t_0}^{t}(\mathbf{x}_0)$ into the tangent space at time t, $T_{\mathbf{x}_t}\mathcal{M}(t)$. By consequence, a unit tangent vector $\mathbf{e}_0 \in T_{\mathbf{x}_0}\mathcal{M}(t_0)$ is also carried into a unit tangent vector $\mathbf{e}_t \in T_{\mathbf{x}_t}\mathcal{M}(t)$ by the flow map;

$$\mathbf{e}_t = \nabla \mathbf{F}_{t_0}^{t}(\mathbf{x}_0)\mathbf{e}_0. \tag{3}$$

The same cannot be said about normal space $N_{\mathbf{x}_0}\mathcal{M}(t_0)$ though, as it is generally not mapped into the normal space $N_{\mathbf{x}_t}\mathcal{M}(t)$. Hence a unit normal vector, $\mathbf{n}_0 \in N_{\mathbf{x}_0}\mathcal{M}(t_0)$, will be of general orientation when mapped ($\nabla\mathbf{F}_{t_0}^t(\mathbf{x}_0)\mathbf{n}_0$). To measure how strongly perturbations in the normal direction grow, Haller (2011) considers the normal component of $\nabla\mathbf{F}_{t_0}^t(\mathbf{x}_0)\mathbf{n}_0$, i.e. its projection into $\mathbf{n}_t$. This parameter is called *repulsion rate* and is defined as:

$$\rho_{t_0}^t(\mathbf{x}_0,\mathbf{n}_0) = \langle \mathbf{n}_t,\ \nabla\mathbf{F}_{t_0}^t(\mathbf{x}_0)\mathbf{n}_0\rangle. \tag{4}$$

$\rho_{t_0}^t(\mathbf{x}_0,\mathbf{n}_0) > 1$ indicates that the infinitesimal normal perturbations applied at time t_0 have grown in the normal direction by time t, and $\rho_{t_0}^t(\mathbf{x}_0,\mathbf{n}_0) < 1$ means these perturbations have diminished by the end of the time interval, and thus, tracking the maximum values of $\rho_{t_0}^t$ close to a boundary corresponds to detecting Lagrangian separation.

Haller (2011) shows that the repulsion rate can also be expressed in terms of the (right) Cauchy-Green tensor $\mathbf{C}_{t_0}^t(\mathbf{x}_0) = \left[\nabla\mathbf{F}_{t_0}^t(\mathbf{x}_0)\right]^\top \nabla\mathbf{F}_{t_0}^t(\mathbf{x}_0)$ as:

$$\rho_{t_0}^t(\mathbf{x}_0,\mathbf{n}_0) = \frac{1}{\sqrt{\langle \mathbf{n}_0,\ \left[\mathbf{C}_{t_0}^t(\mathbf{x}_0)\right]^{-1}\mathbf{n}_0\rangle}}. \tag{5}$$

The finite difference open source code `Incompact3d`, a powerful high-order flow solver for academic research (Laizet & Lamballais, 2009; Laizet & Li, 2011), is used to solve the Navier–Stokes equations. An implicit large eddy simulation, based on the numerical dissipation controlled with the discretization of the viscous term (Dairay *et al.*, 2017), is conducted to obtain a turbulent separation bubble (TSB). The rectangular computational domain has a physical size $1000\theta \times 100\theta \times 50\theta$ in the streamwise x, wall-normal y and spanwise z directions, respectively, where θ is the momentum thickness of the turbulent inlet flow, generated from a previous simulation of a turbulent boundary layer at a Reynolds number $Re_\theta = 800$. A no-slip boundary condition is imposed at the bottom wall ($y = 0$), and along the spanwise direction, the flow is periodic. To generate an adverse pressure gradient, a wall-normal suction velocity profile is imposed using a Gaussian function within a narrow streamwise region on the top wall. An inviscid boundary condition is also applied on the top wall with zero vorticity. A convective boundary condition is finally applied at the outlet section for all velocity components.

RESULTS

To illustrate how the repulsion rate may capture separation before treating the turbulence case, a simulation is performed on a configuration of two solid cylinders of diameter D placed in tandem, separated by a distance of $10D$, and exposed to an incoming flow of constant and uniform velocity U_∞.

The Reynolds number, based on U_∞ and D, reaches $Re = 300$. We place surfaces of particles with the shape of cylinders with a diameter of $1.24D$, initially centered on the solid cylinder axes, and advect them with the non-dimensional time t. The repulsion rate will be calculated based on the deformation of the particles initially located on the material cylinder. Contours of $\rho_{t_0}^{t_0+0.6}$ are plotted for both cylinders at the beginning and the end of the time interval.

On the first cylinder in figure 2, we can clearly see two main quasi-2D separation lines detected on the top and bottom

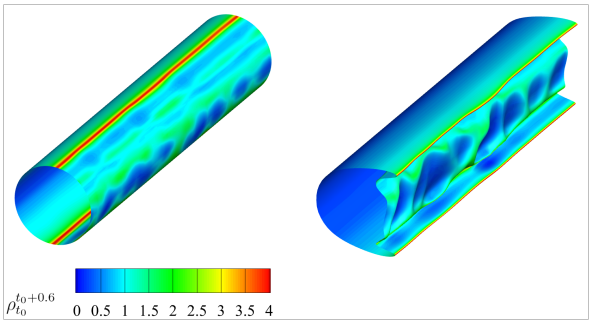

Figure 2. Time evolution of a material surface initially (t_0) centered on the first cylinder axis with a radius of $0.62D$ (*left*), and advected in time until $t = t_0 + 0.6$ (*right*).

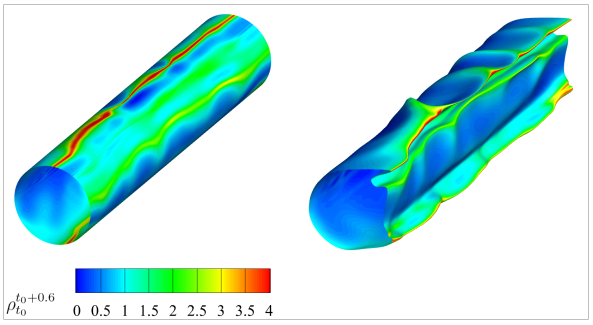

Figure 3. Time evolution of a material surface initially (t_0) centered on the second cylinder axis with a radius of $0.62D$ (*left*), and advected in time until $t = t_0 + 0.6$ (*right*).

sides of the cylinder, which adequately follow the deformed pattern. There are also other patterns on the downstream side of the cylinder, which are captured by the criterion although with a lower value.

The patterns observed on the second cylinder in figure 3 are more complicated and no longer indicate a 2D separation, due to the irregular incoming flow generated by the wake of the first cylinder. Nonetheless, $\rho_{t_0}^{t_0+0.6}$ captures adequately the two main spanwise-oriented separation mechanisms. Some streamwise-oriented separation profiles are also detected with weaker intensity, mainly in the front part of the cylinder.

The lower value areas of repulsion rate in the contours show that the criterion captures separation qualitatively, but additionally measures the strength of separation, i.e. allows to indicate which part of the flow is more susceptible to leave the solid surface.

3D separation patterns of incompressible flows are also investigated by means of the method of Perry & Chong (1986). In this method, a Taylor expansion is assumed for the velocity components up to a desired order. The velocity is then passed along different equations and conditions, and forced to satisfy them (e.g. the continuity equation or the no-slip boundary condition), which simplifies the flow model to an analytically manageable form.

Consider the skin friction field given by equation (6), with y being the wall-normal coordinate, and the skin friction field given by $\tau(x,y,z) = (\tau_x(x,y,z), \tau_z(x,y,z))$:

$$\begin{cases} \tau_x = x^2 + z^2 + 0.1x^3 - 1, \\ \tau_z = -0.5z - xz. \end{cases} \tag{6}$$

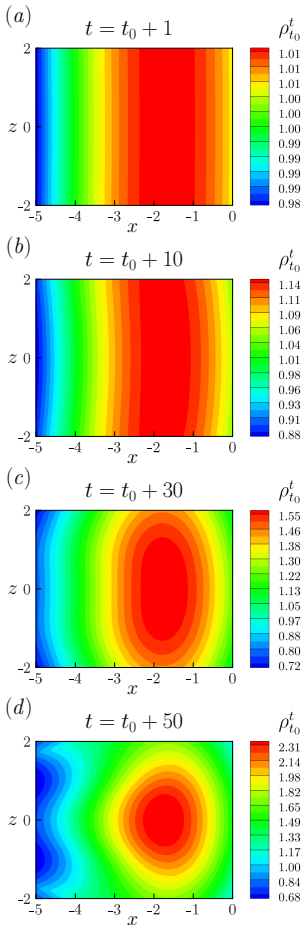

Figure 4. Repulsion rate $\rho^t_{t_0}$ contour on the plane of particles initially located at $y = 0.01$ for the shear stress map (6) and $[t_0, t]$ interval. (*a*) $t = t_0 + 1$. (*b*) $t = t_0 + 10$. (*c*) $t = t_0 + 30$. (*d*) $t = t_0 + 50$.

Particles initially located on a horizontal plane close to the wall (at $y = 0.01$) are advected in time. The repulsion rate is calculated based on the displacement of these particles with time. Figure 4 shows the 2D repulsion rate contours calculated for different durations. These contours are drawn on the initial plane of particles and show $\rho^t_{t_0}$, with t increasing gradually from case (*a*) to (*d*).

As the computation time window increases, the repulsion rate contour becomes more precise and reports more details about the flow. At $t = t_0 + 1$ (case (*a*) of figure 4), the repulsion rate pattern is very simple, with a 2D character, and its value has not considerably deviated from 1.

With time, more relevant patterns become evident and the repulsion rate range increases (evident in the colorbars). At $t = t_0 + 50$ (case (*d*) of figure 4), there are different zones with distinct repulsion rates, each with its own comparative strength. The bolder colors indicate the areas with most growth of perturbations in the normal direction, which is equivalent to particles that take the most distance from the wall in the normal direction (as the plane was initially placed at a constant y location from the surface).

This contour, i.e. $\rho^{t_0+50}_{t_0}$ is studied more closely and the deformation of the initial particles plane located at $y = 0.01$ is followed in figure 5. The steady flow streamlines of the shear stress map (6) are also depicted here. In (*a*), the areas distancing themselves from the wall are properly colored as having the maximum repulsion rate. This is more evident in (*b*) as the surge of particles from the boundary becomes more pronounced. The ridge in the plane of particles is more protruding by the time in (*c*), and we can easily detect the separated area through the criterion. The importance of adequate 3D visualization can be observed through these cases. Further advection of the particles shows that by the time in (*d*), the criterion—computing until $t_0 + 50$, $\rho^{t_0+50}_{t_0}$—remains a good separation indicator even for when particles are convected until $t_0 + 100$. It is evident here that maximum repulsion rate values pertain to the most repelling particles from the wall and the criterion picks up on the particles breaking away from the wall in accordance with the Lagrangian definition of separation.

Figure 6 examines more physical cases and shows the case of a laminar separation bubble (LSB), with an inlet Blasius velocity profile. A material surface, initially aligned with the wall, is advected in time from $t = 0$ and colored with the repulsion rate obtained at $t = 0.25$. With a steady upstream flow, the separation is 2D and occurs on a line oriented in the spanwise direction z. One can see that the repulsion rate reaches its maxima on that line, and therefore captures the Lagrangian separation, however it occurs upstream of the mean Prandtl line visualized with the streamlines of the time- and spanwise-average flow, a phenomenon that was first observed by Haller (2004). In other words, the location of Lagrangian separation differs from its Eulerian counterpart, here illustrated by the Prandtl line usually used to define the mean separation location. Downstream the Prandtl line, several local separation phenomena are also detected, but their analysis is complex. A closer view is proposed in figure 7 for the case of the TSB described in the methodology section. A surface, initially aligned with the wall, is advected in time where the turbulent separation is supposed to occur. The deformed state is complex, but overall, the criterion generally shows a local maximum where particles are the most ejected from the surface.

Results illustrated in figure 6 for the LSB show that applying the general repulsion rate (5) may be difficult in practice as it requires velocity data in space and time, which is even more demanding if a statistical criterion has to be obtained. To overcome this limitation, we investigate the criterion instantaneously by writing a temporal Taylor expansion around the initial time:

$$\rho^{t_0+\Delta t}_{t_0} = 1 + \dot{\rho}_{t_0}\Delta t + O(\Delta t^2), \quad \dot{\rho}_{t_0} := \frac{d}{dt}\rho^{t_0+\Delta t}_{t_0}|_{\Delta t=0}, \quad (7)$$

where $\mathbf{x}_0$ is omitted for clarity. After developments, we obtain

$$\dot{\rho}_{t_0} = \langle \mathbf{n}_0, S\mathbf{n}_0 \rangle, \quad (8)$$

where S is the rate-of-strain tensor. In our geometry, taking material surfaces initially aligned with the bottom wall, equation (8) implies that $\dot{\rho}_{t_0} = \partial v/\partial y = v_y$. Moreover, for incompressible flows where v_y vanishes at the wall, close to the wall, the velocity can be approached by a Taylor expansion in the y direction:

$$v_y(x, y, z) = v_{yy}(x, 0, z)y + O(y^2). \quad (9)$$

On a plane $y > 0$ parallel to the wall, finding the local maxima of v_y is equivalent to finding the local maxima of v_{yy}. Since v_{yy} is a non-zero continuous function in space, this is also the case on the boundary $y = 0$. For 2D flows, a local separation

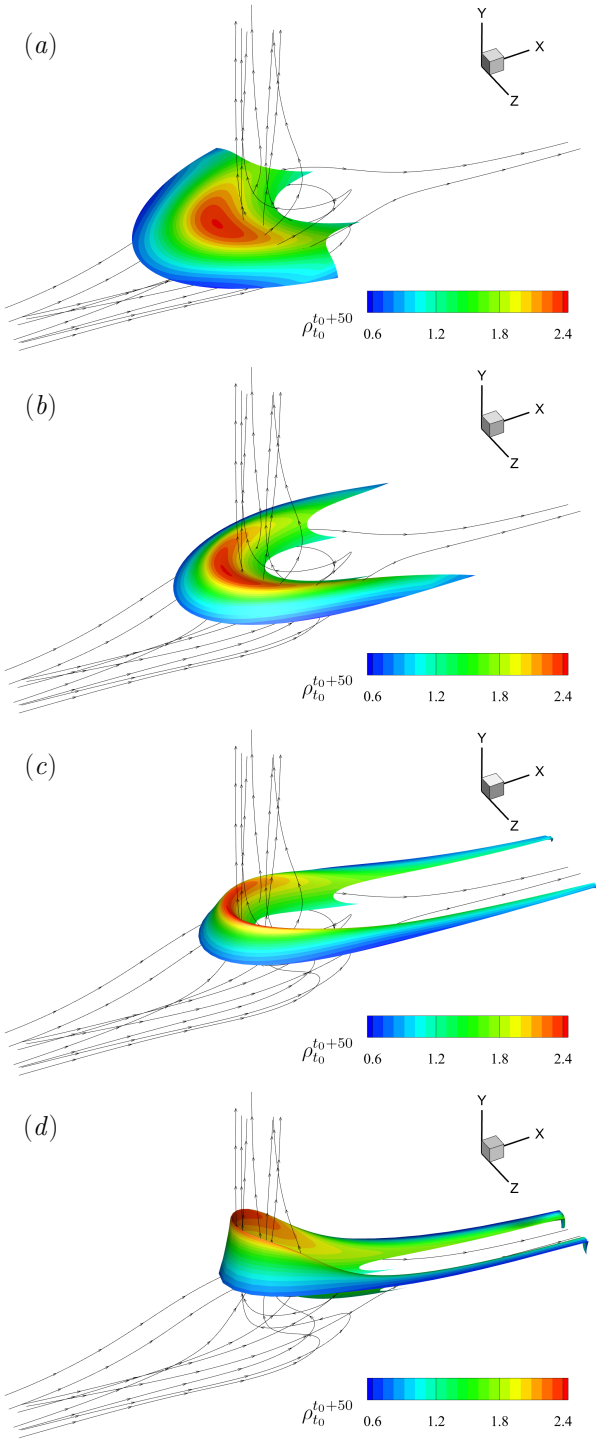

Figure 5. Streamlines and advection of particles for the shear stress map (6), case (*d*) of figure 4. The initially parallel to the wall plane of particles evolves in the flow field. Advection time: (*a*) $t = t_0 + 30$, (*b*) $t = t_0 + 50$, (*c*) $t = t_0 + 70$, (*d*) $t = t_0 + 100$.

point $\mathbf{x}_s = (x_s, 0)$ is then defined where

$$\begin{cases} v_{yyx}(\mathbf{x}_s) = 0, \\ v_{yyxx}(\mathbf{x}_s) < 0. \end{cases} \tag{10}$$

For incompressible flows, the divergence-free velocity vector field allows one to express v_{yy} in terms of skin friction measurements and their spatial derivatives along the wall. Indeed, the skin friction field $\tau = (\tau_x, \tau_z) = (\mu\, u_y, \mu\, w_y)$ in the xz plane can be utilized to find an alternative relation for the instantaneous repulsion rate. From continuity:

$$\begin{aligned} v_{yy} &= -u_{xy} - w_{zy} \\ &= -\frac{1}{\mu}\left(\partial_x \tau_x + \partial_z \tau_z\right) \\ &= -\frac{1}{\mu}\nabla_{||} \cdot \tau, \end{aligned} \tag{11}$$

where $\nabla_{||} = \mathbf{e}_x\, \partial_x + \mathbf{e}_z\, \partial_z$, with $\mathbf{e}_x$ and $\mathbf{e}_z$ unit vectors in the x and z directions, respectively. Hence the repulsion rate derivative is also proportionate to the divergence of the wall skin friction field.

We use (11) in the case of the TSB to capture the birth of separation. In the top-right corner of figure 7 is plotted the evolution of $\dot{\rho}_{t_0}$, averaged over time and spanwise direction. Statistically, the results show that the mean Lagrangian separation occurs, just like the LSB, upstream of what is usually accepted as the definition of the mean separation point/line represented by the Prandtl criterion (visible with the streamlines). In the same plot, the evolution of the forward flow fraction γ, which represents the percentage of time that the longitudinal velocity is positive, is also shown. While the mean separation point can be captured with $\gamma = 50\%$, $\dot{\rho}_{t_0}$ indicates that the Lagrangian criterion is localized upstream, close to what is called the incipient detachment (Simpson, 1996), where the forward flow fraction is 99%.

CONCLUSION

Traditional criteria based on Eulerian quantities are still extensively used today to detect flow separation, as for example in aerodynamics. For numerical simulations, most of DNS/LES results extract separation by generally capturing the Prandtl criterion on spanwise-averaged data (a periodic boundary condition in that direction is systematically used). However, this is Lagrangian separation that is visualized in experiments when particles are used to seed the flow. Here we show that the location of the mean Lagrangian separation clearly and strongly differs from what is generally known as the mean separation point, obtained from the vanishing mean wall-friction point. In the domain of flow control, this indicates that the effort to reduce separation based on focusing on the mean separation point/line could be revisited.

REFERENCES

Dairay, T., Lamballais, E., Laizet, S. & Vassilicos, J. C. 2017 Numerical dissipation vs. subgrid-scale modelling for large eddy simulation. *Journal of Computational Physics* **337**, 252–274.

Haller, G. 2004 Exact theory of unsteady separation for two-dimensional flows. *Journal of Fluid Mechanics* **512**, 257–311.

Haller, G. 2011 A variational theory of hyperbolic Lagrangian Coherent Structures. *Physica D: Nonlinear Phenomena* **240** (7), 574–598.

Laizet, S. & Lamballais, E. 2009 High-order compact schemes for incompressible flows: A simple and efficient method with quasi-spectral accuracy. *Journal of Computational Physics* **228** (16), 5989–6015.

Laizet, S. & Li, N. 2011 Incompact3d: A powerful tool to tackle turbulence problems with up to $O(10^5)$ computa-

tional cores. *International Journal for Numerical Methods in Fluids* **67** (11), 1735–1757.

Moore, F. K. 1958 On the separation of the unsteady laminar boundary layer. In *Boundary-layer Research* (ed. H. Görtler), pp. 296–311. Berlin, Heidelberg: Springer.

Perry, A. E. & Chong, M. S. 1986 A series-expansion study of the Navier–Stokes equations with applications to three-dimensional separation patterns. *Journal of Fluid Mechanics* **173**, 207–223.

Prandtl, L. 1904 Über Flüssigkeitsbewegung bei sehr kleiner Reibung. *Verh. III, Intern. Math. Kongr. Heidelberg* **2**, 484–491.

Rott, N. 1956 Unsteady viscous flow in the vicinity of a stagnation point. *Quarterly of Applied Mathematics* **13** (4), 444–451.

Santhosh, S., Qin, H., Klose, B. F., Jacobs, G. B., Vétel, J. & Serra, M. 2023 Spike formation theory in three-dimensional flow separation. *Journal of Fluid Mechanics* **969**, A25.

Sears, W. R. 1956 Some recent developments in airfoil theory. *Journal of the Aeronautical Sciences* **23** (5), 490–499.

Serra, M., Vétel, J. & Haller, G. 2018 Exact theory of material spike formation in flow separation. *Journal of Fluid Mechanics* **845**, 51–92.

Simpson, R. L. 1996 Aspects of turbulent boundary-layer separation. *Progress in Aerospace Sciences* **32** (5), 457–521.

Surana, A., Grunberg, O. & Haller, G. 2006 Exact theory of three-dimensional flow separation. Part 1. Steady separation. *Journal of Fluid Mechanics* **564**, 57–103.

Surana, A., Jacobs, G. B., Grunberg, O. & Haller, G. 2008 An exact theory of three-dimensional fixed separation in unsteady flows. *Physics of Fluids* **20** (10), 107101.

Van Dommelen, L. L. & Shen, S. F. 1980 The spontaneous generation of the singularity in a separating laminar boundary layer. *Journal of Computational Physics* **38** (2), 125–140.

Van Dommelen, L. L. & Shen, S. F. 1982 The genesis of separation. In *Numerical and physical aspects of aerodynamic flows* (ed. T. Cebeci), pp. 293–311. Springer.

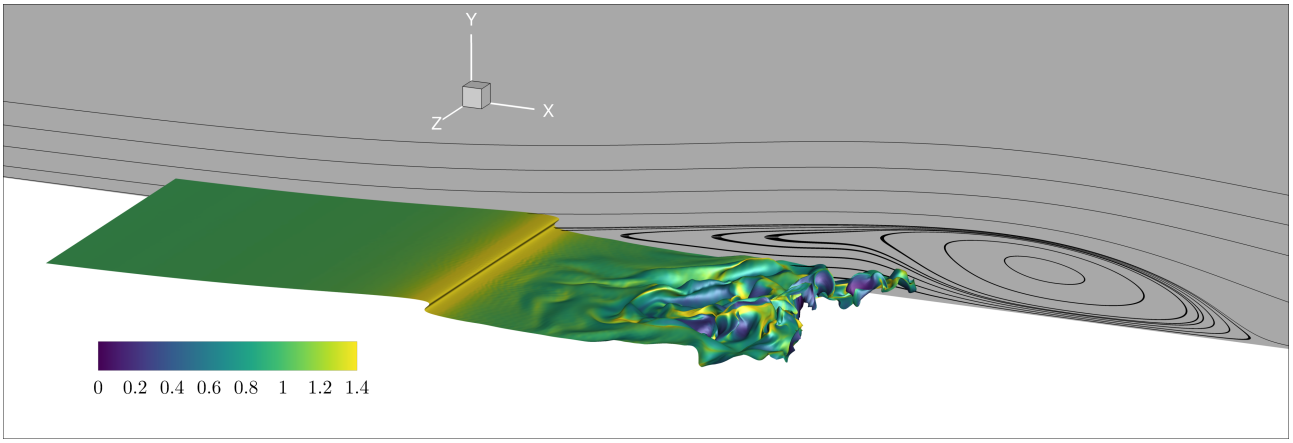

Figure 6. Time evolution of a material surface initially tangent to the bottom wall colored by $\rho_0^{0.25}$ in the case of a laminar separation bubble. The vertical plane shows streamlines of the time- and spanwise-averaged flow.

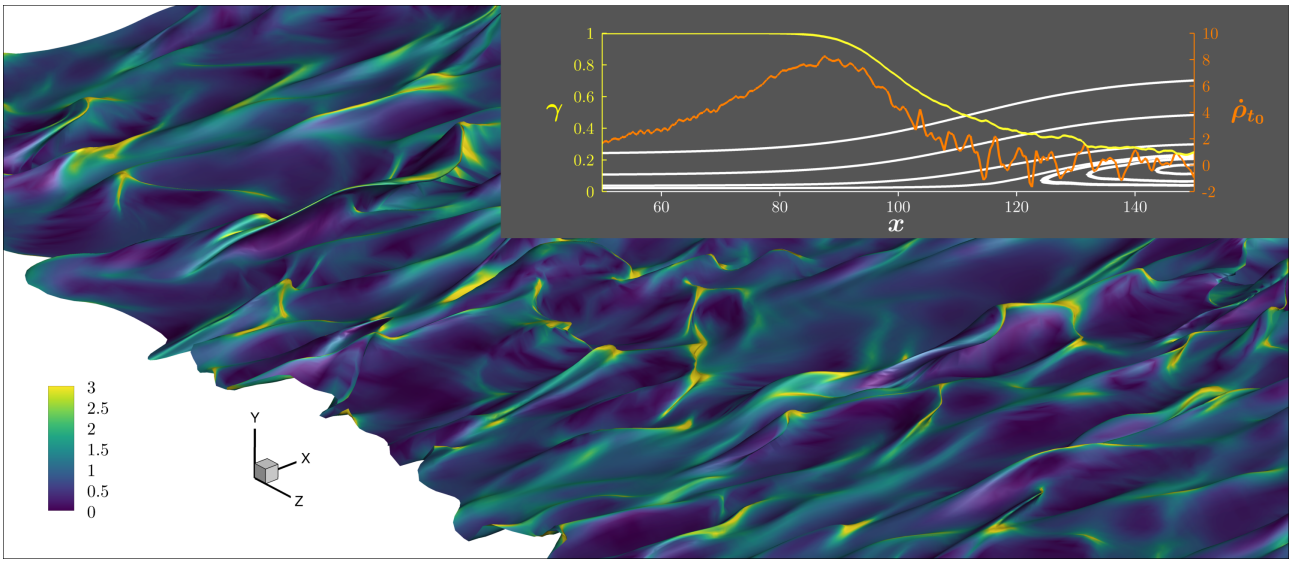

Figure 7. Time evolution of a material surface initially tangent to the bottom wall colored by ρ_0^4 in the case of a turbulent separation bubble. The deformed surface originally begins at $x = 70$ for $t = 0$. In the top right corner are plotted some streamlines (white) of the time- and spanwise-averaged flow in the vicinity of the mean separation point, together with the evolution of the forward flow fraction γ (yellow) and the instantaneous repulsion rate $\dot{\rho}_{t_0}$ along the $y = 0$ axis.